Pore-scale visualization and characterization of viscous dissipation in porous media

Sophie Roman, Cyprien Soulaine, Anthony Kovscek

Contents lists available at ScienceDirect

Journal of Colloid and Interface Science

journal homepage: http://ees.elsevier.com

Pore-scale visualization and characterization of viscous dissipation in porous media

Sophie Roman [a,c,*], Cyprien Soulaine [a,b], Anthony R. Kovscek [c]

[a] Université d'Orléans/CNRS/BRGM, UMR 7327, 1A rue de la Férollerie, 45100 Orléans, France
[b] BRGM, 3 Avenue Claude Guillemin, 45100 Orléans, France
[c] Department of Energy Resources Engineering, Stanford University, Stanford, CA 94305, USA

ARTICLE INFO

Article history:
Received 10 June 2019
Received in revised form 19 September 2019
Accepted 20 September 2019
Available online xxx

Keywords
Porous media
Two-phase flow
Microfluidics
Capillary forces
Viscous coupling

ABSTRACT

Hypothesis: The effects of mutual transfer of momentum between two immiscible flowing fluids in porous media is not well understood nor predictable yet. From considerations at the pore-scale, it should be possible to determine whether and to what extent interfacial viscous coupling effects are significant.
Experiments: We visualize the velocity distributions inside immobile globules of wetting phase (water) while a non-wetting phase (oil) is injected. We investigate viscous coupling effects and their relationship with the viscosity ratio and the capillary number.
Findings: Four regimes of viscous dissipation are identified: (i) a regime for which the fluid-fluid interface acts as a solid wall; (ii) a regime where the wetting phase is dragged in the direction of the imposed flow; (iii) and (iv) two regimes for which the trapped globule of water shows a recirculating motion due to the shear stress at the oil/water interface. We demonstrate the significant role of the lubricating effect and of the topology of the pore space on the magnitude of viscous dissipation. Importantly, for a viscosity ratio close to one and low capillary number, we demonstrate that viscous coupling effects should be incorporated into the existing Darcy's law formulation for two-phase flow in porous media.

1. Introduction

Multiphase flow in porous media is important in a number of environmental and industrial subsurface applications such as the sequestration and storage of CO_2 in geological formations [1], enhanced oil recovery [2], soil remediation [3], and energy storage technologies. Interest also extends to manufactured porous materials such as nuclear safety devices [4], and distillation columns [5]. In particular, a fundamental understanding of the mechanisms of displacement of one fluid by another in porous media is crucial to predict optimal hydrocarbon recovery and subsurface storage of CO_2. An accurate description of the flow mechanisms in porous media, however, is challenged by the complex interplay between capillary, viscous and gravitational forces that may lead to highly unstable flows and trapping mechanisms. The heterogeneous nature of geological formations further complicates the development of predictive models.

The common approach to describe immiscible two-phase flows in porous media is to consider a heuristic extension of Darcy's law for multiphase systems –also referred to as the generalized Darcy's law– by introducing concepts such as fluid saturation, relative permeability, and capillary pressure [6]. In this model, the velocity of each phase is governed by Darcy's law where the rock permeability is weighted by a function known as the relative permeability that accounts for a space reduction due to the presence of the other fluid phase. Despite a very large usage in the subsurface engineering community, a number of studies have emphasized the limits of this model [7–9]. For example, investigations of unstable two-phase flow at the core-scale [10] have demonstrated that the flow processes are not described adequately by the generalized Darcy's law. This is not surprising given that this model relies upon strong assumptions, including a locally stable fluid-fluid interface at the pore-scale [11], as well as separation of scale between the local events and the large-scale phenomena. More importantly, the standard multiphase Darcy approach assumes that the shear stress exerted at the fluid-fluid interface does not impact large-scale behavior [12]. In the standard multiphase version of Darcy's law, each fluid interacts with respect to each other as if all interfaces are no slip. That is, the tangential velocity of the fluid-fluid interface is assumed to be zero. Hence, the mutual interactions between the fluids are neglected.

The range of validity of Darcy's law extended for two-phase systems is therefore limited to systems with large viscosity ratio [9] or when the interfacial area between the two fluids is small. The latter point is not necessarily valid in situations where multiple phases coexist within one pore, e.g. in presence of films at the solid walls or in very perme-

* Corresponding author at: Université d'Orléans/CNRS/BRGM, UMR 7327, 1A rue de la Férollerie, 45071 Orléans, France.
E-mail address: sophie.roman@univ-orleans.fr (S. Roman)

https://doi.org/10.1016/j.jcis.2019.09.072
0021-9797/

able media where the pore size is large enough to have unsaturated pores. The assumptions behind Darcy's law extended to multiphase flows break down for many systems of interest. For example, the viscosity ratio, $M = \mu_{nw}/\mu_w$, where *nw* is for non-wetting and *w* for wetting, of sCO_2/brine systemsis about 0.10 [13], M is about 1.00 for LNAPL(Light Non-Aqueous Phase Liquid, e.g. gasoline)/groundwater systems [14], about 3.00 for DNAPL (Dense NAPL, e.g. aromatic hydrocarbons)/groundwater systems [15] and M is about 10.00 for crude oil/brine systems [16].

For more than 60 years a number of authors have questioned the validity of the standard multiphase Darcy approach, specifically whether viscous coupling or lubrication of a non-wetting phase by a wetting film is significant [16,17]. Indeed, the effect of viscous coupling and lubrication is associated with the mobility of the phases and with the dissipation of mechanical energy [18,19]. The details of the process of thin film deposition on solid surfaces by a moving meniscus have received a lot of attention. The lubrication effects depend on both the flow rate and the wetting properties of both fluids and the solid surface [20,21]. Recent theories and experimental characterization are still being developed to describe unexplored lubrication regimes [22–24]. Although, one of the most highlighted phenomena, the lubrication effect, however, is not the only source of viscous dissipation. For example, the mutual interaction between an immobile and a flowing fluid can increase the mobility of the flowing phase [7,17]. This situation is expected in applications such as the storage of CO_2 in deep saline aquifers. Indeed, after the injection of CO_2 into the subsurface, a large number of ganglia of supercritical CO_2 is immobilized in the porous matrix of the geological formations [25–27].

In a former study, Roman et al. [28] investigated this configuration using analog fluids during drainage experiments in a sandstone-replica micromodel. The authors observed that the macroscopically immobile pockets of wetting fluid in the porous matrix show a recirculating motion due to the shear stress resulting from the displacement of the other phase, similar to the well-known driven cavity flow. These direct visualizations were realized using the micro-PIV (Particle Image Velocimetry) technique developed to measure the velocity fields within an aqueous phase during micromodel experiments [28]. The evidence of slip boundary conditions at the fluid/fluid interface and of eddy swirl of the trapped phase has been confirmed later by others [29,30]. For viscous dominated regimes, Heshmati and Piri [29] observed the same phenomenon of fluid/fluid interactions using a two-phase and two-fields of view micro-PIV setup. Recently, using microfluidics experiments, Zarikos et al. [30] studied the drag force exerted on the fluid-fluid interface between a trapped globule and a flowing phase to understand the mobilization of the globules. These experimental works clearly emphasize the existence and importance of interfacial viscous coupling effects. The magnitude of these events, however, has not been evaluated nor related to a macroscale description of the flow.

The significant advance in this manuscript is a detailed study of the viscous coupling effects and the flow mechanisms that produce them with the overall goal of developing a satisfactory quantitative macroscale model [31]. By performing a detailed study of viscous coupling effects between an immobile and a flowing phase, this paper explores the origins of dissipative processes at the pore-scale during the drainage of a wetting fluid displaced by a non-wetting phase, as a function of the flow parameters, and then evaluates the consequences of the fluid/fluid interactions at larger scales. For this purpose, two-phase flow microfluidic experiments are performed in simplified and very well-controlled pore geometries. These micromodels are designed to focus on the trapping mechanisms in cavities bounding a capillary throat. The velocity fields and the distribution of the local dissipation of mechanical energy within trapped globules are analyzed using micro-PIV for various flow conditions and fluid parameters (i.e., interfacial area, viscosity ratio, interface velocity etc.). Different regimes of fluid/fluid interaction between a trapped and a flowing phase are highlighted and discussed. We identified that the viscosity ratio, the lubrication effect, and the shape of the immobile globule play an important role in describing viscous coupling effects during immiscible two-phase flows.

The paper is organized as follows. First, we describe the theoretical background of multiphase flow in porous media. Second, we present the experimental setup and the method developed to analyze the flow behaviors. Then, we present the local velocity profile within wetting phase globules immobilized by capillarity, and we discuss its implication at larger scale. Finally, we conclude and propose some perspectives of this work.

2. Theoretical background: continuum-scale model

In this section, we expose the theoretical background of two-phase flows at the continuum scale, focusing on the drag forces. The aim is to provide a means to evaluate the magnitude of the momentum transfer force at the fluid-fluid interface. Importantly, we provide insights to evaluate the importance at the continuum scale of viscous coupling during two-phase flow from pore-scale experiments.

In two-fluid models, each phase is treated separately with its own conservation equations describing the balance of mass and momentum. Without any *a priori* assumption on the formulation of the drag forces, the integration of the two-phase Stokes momentum equations over a representative elementary volume, V, of the porous medium gives [32–34],

$$\begin{cases} 0 &= -\phi_o \nabla P_o + \boldsymbol{M}_{os} + \boldsymbol{M}_{ow} \\ 0 &= -\phi_w \nabla P_w + \boldsymbol{M}_{ws} - \boldsymbol{M}_{ow} \end{cases} \tag{1}$$

where $\phi_i = \frac{V_i}{V}$ is the volume fraction of phase i, P_i is the macroscale pressure field of phase i, $\boldsymbol{M}_{is}$ is the drag force exerted by fluid i onto the solid surface normalized by the volume V, and $\boldsymbol{M}_{ow}$ is the mutual momentum transfer between the wetting phase and the non-wetting phase. The drag force, $\boldsymbol{M}_{ij}$, of fluid i relative to phase j is written as

$$\boldsymbol{M}_{ij} = \frac{1}{V}\int_{A_{ij}} \boldsymbol{n}_{ij}.\sigma_i dA \tag{2}$$

where $\boldsymbol{n}_{ij}$ is the normal vector at the interface pointing from the fluid i to the phase j, $\int_{A_{ij}} dA$ is the sum over the surface area of the interface, and σ_i is the local stress tensor given by,

$$\sigma_i = -p_i \mathrm{I} + \mu_i \left(\nabla \boldsymbol{u}_i + \nabla^t \boldsymbol{u}_i\right) \tag{3}$$

where p_i, $\boldsymbol{u}_i$, and μ_i are the local pressure, the local velocity profile and the viscosity of fluid i, respectively.

The formulation of the two-phase macroscale model introduced in Eqs. (1) and (2) is generic and offers an appealing framework to interpret the pore-scale flow patterns. According to the constitutive relations used to relate the drag forces to the mean velocity, $\boldsymbol{U}_i$, of phase i, Eq. (1) can be rewritten in terms of the standard generalized Darcy's law or as alternative models. For example, assuming that the total drag force exerted by the fluid o onto both the solid surface and the fluid-fluid interfacial area is related to the phase average velocity $\boldsymbol{U}_o$ by $\phi_o^{-1}\left(\boldsymbol{M}_{os} + \boldsymbol{M}_{ow}\right) = -\mu_o \mathsf{K}_{ro}^{-1}.\phi_o \boldsymbol{U}_o$ and that the drag force exerted by the other fluid onto its bounding surface area is $\phi_w^{-1}\left(\boldsymbol{M}_{ws} - \boldsymbol{M}_{ow}\right) = -\mu_w \mathsf{K}_{rw}^{-1}.\phi_w \boldsymbol{U}_w$, then the two-fluid model, Eq. (1), becomes the generalized Darcy's law [6] where each phase is governed by a Darcy's law, $\phi_i \boldsymbol{U}_i = -\frac{\mathsf{K}_{ri}}{\mu_i}\nabla P_i$. In these equations, K_{ri}, known as relative permeability, is the skin factor of the drag force applied by fluid i onto its bounding surface, regardless the nature of the surface (fluid or solid). These closure equations, however, imply that the fluid-fluid interface is immobile, which is not necessarily a correct statement as ob-

served. Indeed, experimental measurements using the micro-PIV technique emphasize a tangential motion of the fluid/fluid interface [28–30].

A more flexible approach for describing the multiphase drag forces is to write $\boldsymbol{M}_{os} = \mathsf{A}_{os}.\boldsymbol{U}_o$, $\boldsymbol{M}_{ws} = \mathsf{A}_{ws}.\boldsymbol{U}_w$ and $\boldsymbol{M}_{ow} = \mathsf{A}_{ow}.\left(\boldsymbol{U}_o - \boldsymbol{U}_w\right)$ where A_{ij} are some closure coefficients that depend on the fluid viscosities and the interfacial area between the phases i and j. The combination of these constitutive relations and the two-fluid model leads to equations with mutual momentum transfer due to viscous forces at the interface between the two flowing fluids [35,36]. With some simple algebra, this model can be recast into the two-phase Darcy equations with coupling terms [37–39], $\phi_i \boldsymbol{U}_i = -\frac{\mathsf{K}^*_{io}}{\mu_o}\nabla P_o - \frac{\mathsf{K}^*_{iw}}{\mu_w}\nabla P_w$ where the four K^*_{ij} tensors are commonly referred to as generalized relative permeability coefficients. It is not clear whether or not these tensors depend on the viscosity ratio and what is the exact physical meaning of such parameters. The four generalized relative permeability tensors are actually dependent on each other [38] and the number of unknowns is reduced to three, namely A_{os}, A_{ws} and A_{ow}. There have been several attempts to determine the four coupling tensors experimentally, for example Kalaydjian [40], Rose [37], Dullien and Dong [41] showed that the coupling coefficients are important for a range of flow systems in porous media whereas Zarcone and Lenormand [12] concluded that viscous coupling can be neglected for continuous fluid phases with large interfacial tension. Techniques have been developed to measure the generalized coefficients, however they are very different from one another and the reliability of the obtained results are in many cases questionable [42]. Using a Lattice Boltzmann model Li et al. [42] have shown that viscous coupling is important, they found strong correlation between the relative permeability and the interfacial area between fluids. For Li et al. [42], this indicates that both the standard two-phase Darcy approach and the generalized formulation accounting for viscous coupling effects do not provide satisfying insight into two-phase flow processes in porous media. Numerically, Shams et al. [43] studied viscous coupling effects in two-phase flow through non-circular capillary tubes. Their results indicate that momentum transfer across the interface can significantly affect the mobility of fluid layers that form in corners of a capillary. In conclusion, the importance of the viscous coupling terms has been demonstrated for a number of flow configuration, however, they still need to be understood and characterized for a large range of flow conditions.

In the following, we will not speculate the form of the drag forces but we keep the generic formulation introduced in Eq. (1). Using flow measurements, directly at the pore-scale, we evaluate the magnitude of the interfacial momentum transfer force, $\boldsymbol{M}_{ow}$, for different flow conditions.

3. Material and methods

In this section we describe our experimental setup and the measurement techniques that we developed to investigate internal flow and momentum transfer within immobile wetting phases in micromodels.

3.1. Micromodels

The experimental apparatus includes micromodels connected to a flow controller and placed under a microscope for flow visualization. The micromodels contain an etched flow pattern that enables the visualization of fluid movement at the pore-scale. Fig. 1 presents the experimental setup with the micromodel geometries used. Different micromodel patterns are employed: (i) microchannels containing constrictions as a model of successive pore body/pore throat, (ii) microchannels containing eddy pockets as a model of dead-end pores where a fluid can be trapped, and (iii) micromodels representing a pore-doublet. These different geometries represent various pore-throat and pore-body configurations of interest for porous systems. The size of the microchannels, the ratio between the size of the pore throat and the pore

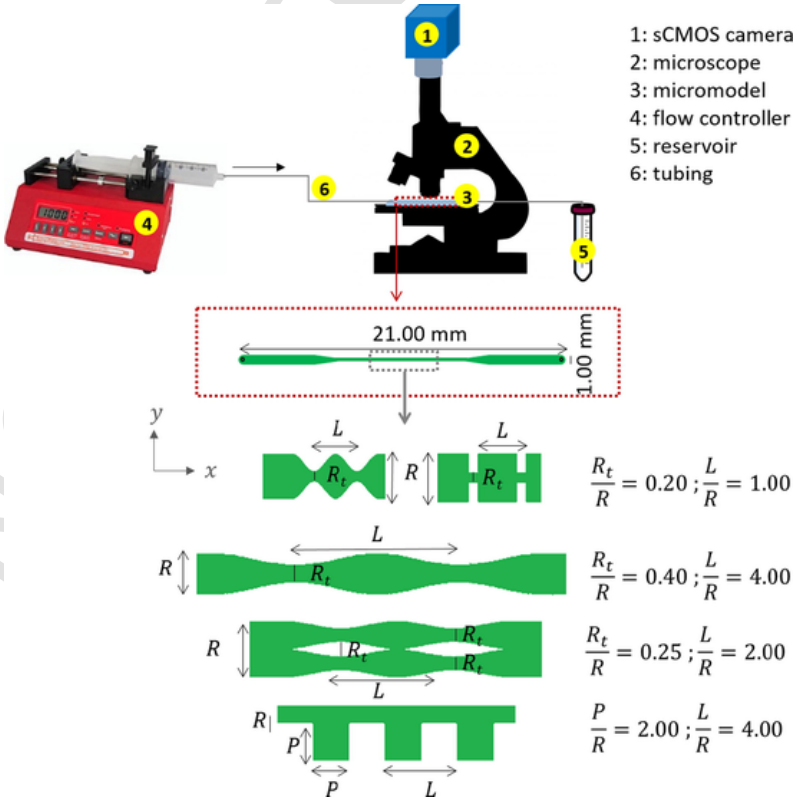

Fig. 1. Experimental setup and geometries of the etched patterns. The size of the pore body R is 100.00 microns for all geometries. The depth of the channels is about 35.00 microns.

body, and the ratio between the size of the channel and the size of the pocket are varying. The pore sizes are typical of natural porous media, i.e. pore body a hundred microns, pore throat tens of microns. The depth of the pores is uniform along the microchannels and is about the size of the pore throats. The microchannels are 4 mm long and connected to larger microchannels for fluid delivery and production.

Two types of micromodels were fabricated: silicon/glass and PDMS (Polydimethylsiloxane) micromodels. The geometrical characteristics of PDMS features are not as well controlled as for silicon-etched micromodels, however, PDMS micromodels have advantages of being easy, cheap, and quick to fabricate. Thus, for larger features PDMS was preferred to silicon. For silicon/glass micromodels, the protocol is the same that we used in Roman et al. [28] and is detailed in Hornbrook et al. [44] and Buchgraber et al. [45]. Briefly, the pattern is etched onto silicon using standard photolithography techniques. Holes are drilled into the silicon wafer for connection to the fluidic system. After cleaning, the wafer is bonded to a glass plate. The silicon is oxidized during bonding, and results in a water wet surface layer. For PDMS microfabrication, first a mold in silicon containing the positive relief of the microchannels is fabricated by photolithography. The mold is then used for the PDMS molding process. A cast of the channels is obtained by pouring transparent liquid PDMS (Silicone Elastomer, Sylgrad) onto the mold, baking it (1 h, 65 °C), and removing it from the wafer. Holes for the fluids interconnections are then drilled in the PDMS. Another cast of PDMS is prepared by pouring liquid PDMS into a flat mold. Before bonding, the two PDMS layers are cleaned with ethanol in an ultrasonic bath. An oxygen plasma treatment is applied to both PDMS layers in order to activate their surface, then they are bonded. To overcome the intrinsic hydrophobicity of PDMS, before an experiment a second extended plasma treatment (5.00') is applied to the device to allow the PDMS surface to remain hydrophilic for more than 5 h [46].

3.2. Fluidics and imaging

A constant injection rate (from 5.00×10^{-4} to 1.00×10^{-1} mL/ min) is provided by a syringe pump (Harvard Apparatus Pump 11 Elite). The syringe (Stainless Steel Syringe, Swagelock®) contains water or oil. For flow visualization, a Nikon Eclipse microscope is used. The light source is a Metal Halide lamp, and a camera (pco.edge or Andor Neo, sCMOS 5.50 Megapixel, up to 500 fps) is used to acquire sequences of images.

Drainage experiments are performed using different fluid pairs. The wetting fluid is DI water or a mixture of DI water and glycerol to modify the viscosity. For the non-wetting phase, we use decane (Sigma Aldrich) or silicone oil (5 cSt Sigma Aldrich), depending on the viscosity ratio, $M = \frac{\mu_{oil}}{\mu_{water}}$, targeted. The properties of the fluid pairs are detailed in Table 1. Estimates of the interfacial tensions are found in the literature [9,29,47]. For micro-PIV measurements, the wetting phase is seeded with polystyrene micro-particles (Polybead Carboxylate Microsphere 1 μm diameter, Polyscience). The seeding concentration is set at approximately 0.06 % by volume.

3.3. Image processing and micro-PIV

Using the experimental setup described above we record sequences of images of particle and fluid/fluid interface displacement. An image processing workflow was developed using the MATLAB® Image Processing Toolbox that results in a set of sequences of images containing only information related to the moving particles that are then used for micro-PIV measurements. Another set of images contains information related to the moving or static fluid/fluid interface. More details on image processing can be found in Roman et al. [28].

Particle Image Velocimetry (PIV) is a widely used technique that allows mapping of the flows in a fluid. In Roman et al. [28] we provided a careful analysis and validation of micro-PIV measurements during two-phase flows in micromodels. For standard PIV measurements fluorescence imaging is used where a laser sheet incident on the fluid flow reflects off the particles and scatters towards a camera. In our setup, optical images of the moving particles are recorded with a camera. Thus, we rely upon effective image processing prior to PIV measurements [28]. Micro-PIV measurements are performed using PIVlab, a MATLAB® tool [48].

3.4. Experimental procedure, measurements and post-processing

The aim of this work is to understand the importance of viscous dissipation mechanisms, and to find out the relationship between viscous dissipation, interfacial area, viscosity ratio, surface tension, etc. For that, we perform drainage experiments in simple and very well controlled geometries in order to have a control over all the flow parameters. A typical experiment is made of the following sequence of events. First, the micromodel is saturated with the wetting fluid (water). Then, the non-wetting fluid (oil) is injected at a constant flow rate, and the passage of the oil front and the movement of trapped pockets of wetting phase (where applicable) are recorded. Finally, the records are analyzed using image processing to obtain several micro- and macro-scale flow parameters.

The analysis of the phase distribution leads to the measurement of the volume (actually a surface area because the microfluidic measurement are performed in 2D from the top view) V_w of wetting fluid, and the area A_{wo} of the oil-water interface.

The 2D velocity field in immobilized wetting phase pockets, $u(x,y)$, is obtained from the micro-PIV measurements, as illustrated in Fig. 2. The symmetrical strain rate tensor, e_{ij}, defined as

$$e_{ij} = \frac{1}{2}\left(\frac{\partial u_j}{\partial x_i} + \frac{\partial u_i}{\partial x_j}\right), \tag{4}$$

is, then, computed to define the viscous stress along the interface,

$$T = \int_{A_{wo}} 2\mu_w e_{ij}.\mathbf{n}dA, \tag{5}$$

where $\mathbf{n}$ is the normal to the oil-water interface. Note that the effect of the local pressure is neglected to calculate the shear stress at the fluids interface because for the range of parameters considered experimen-

Table 1
Properties of experimental fluid pairs at room pressure and temperature (25 °C and 1 atm).

Fluid pair #	Wetting (w)	Non-wetting (nw)	Viscosity μ_w (mPa s)	Viscosity μ_{nw} (mPa s)	Viscosity ratio $M = \frac{\mu_{nw}}{\mu_w}$	Interfacial tension (mN/m)
1	DI water	Decane	0.89	0.83	0.93	≈ 50
2	DI water	Silicone oil 5 cSt	0.89	4.60	5.20	≈ 35
3	50% DI water/50% glycerol	Silicone oil 5 cSt	5.10	4.60	0.90	≈ 20
4	20% DI water/80% glycerol	Silicone oil 5 cSt	49.00	4.60	0.09	≈ 15

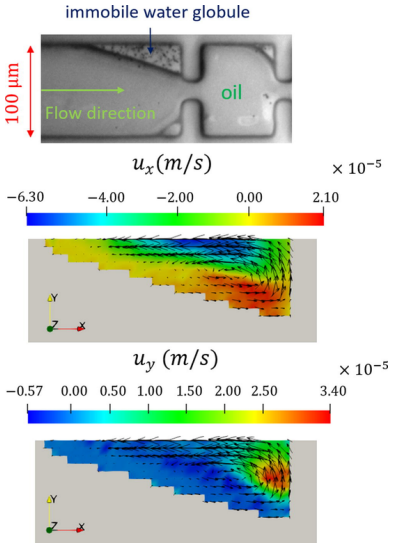

Fig. 2. Immobile pocket of water and velocity fields measured using micro-PIV.

tally the viscous forces dominate over inertial forces [49]. The drag force M_{ow} involved in Eq. (1) is related to the shear stress T using

$$M_{ow} = \frac{T \times A_{wo}}{V}, \tag{6}$$

with V a representative elementary volume.

We use Pilotti et al. [18] formulation to calculate the local rate of viscous dissipation of mechanical energy per unit mass of fluid,

$$\varphi = \frac{2\mu_w}{\rho_w} e_{ij} e_{ij}, \tag{7}$$

The mean rate of dissipation of mechanical energy is obtained by integrating φ over each wetting phase pocket and dividing by the volume, V_w, of the pocket:

$$\Phi = \frac{1}{V_w} \int_{V_w} \varphi dV. \tag{8}$$

We also use dimensionless numbers to characterize the macroscale parameters and identify different flow regimes. The viscosity ratio between oil (o) and water (w), M, is defined as,

$$M = \frac{\mu_o}{\mu_w}, \tag{9}$$

and the capillary number, Ca, that determines the importance of surface tension forces with respect to viscous forces, is calculated as

$$Ca = \frac{\mu_w V_o^I}{\sigma}, \tag{10}$$

where V_o^I is the velocity of the oil/water interface at the center of the inlet channel and σ is the oil/water interfacial tension.

4. Results and discussion

In this section we present and discuss measurements of the velocity fields, energy dissipation, and drag force inside an immobile pocket of aqueous phase during drainage. First we present results of the eddy pocket model for two-phase flow. Then we show measurements for various pore geometries for which we identify different regimes of viscous dissipation. Finally we discuss the experimental results.

4.1. Eddy pocket micromodels

In this section, we describe the flow mechanisms observed during drainage in the dead-end pore micromodels (i.e. eddy pockets). Unlike the other channel geometries, here we know that trapping occurs in the dead-end pore with similar immobilized wetting fluid shape for all experiments. Moreover, as theoretical works are based on similar channel geometries [17,50], they are used to compare with our observations.We performed drainage experiments for eddy pocket micromodel geometry with the fluid pairs 2, 3 and 4 listed in Table 1 to observe how the internal flow behavior varies with the fluid properties and flow conditions characterized by the dimensionless numbers Ca and M.

The flow pattern and the velocity of the oil/water interface during oil invasion in the microchannel is presented in Fig. 3 for the case of fluid pair 4. The velocity of the interface is measured at the center of the inlet channel. The interface velocity decreases as the interface is entering a pocket of wider cross-section. The evolution of the interface velocity along the x-axis of the channel shows a periodic pattern following the successive pockets. The pattern of the advancing interface is similar for all the drainage experiments in eddy pocket micromodels. For the series of experiments that we performed, the velocity magnitude and the depth of penetration of the oil in the pockets changes with Ca and M. The shape of the fluid/fluid interface in the vicinity of the pocket is more complicated than the flat curvature assumed by W. Rose in his pseudo-analytical model [17]. Recently, Liu et al. [50] studied the effect of the viscosity ratio, shear stress and external pressure gradient on lubricant retention using micromodels experiments and a theoretical model with a channel geometry similar to the eddy pockets presented in this work. Interestingly, they are able to predict the steady-state deformation of the fluid-fluid interface in the pocket that depends on the viscosity ratio and on the non-wetting phase flow rate. The results of Liu et al. [50], however, are limited to high flow rates, and the width of the inlet channel is much wider compared with the pocket depth. In a future work it would be interesting to adapt their theoretical model and compare it with our measurements.

After the passage of the oil interface, the wetting phase held in the pockets is either quiescent or shows a recirculating motion that continues as long as oil is injected at a constant flow rate. In some cases, the trapped pocket is continuously fed by water films flowing along the walls, while in other cases, the trapped water is completely disconnected from the main flow. Visually the patterns of the oil invasion as seen on Fig. 3 are very similar for all experiments, whether we observe a recirculating motion in the water phase after invasion or not. The only difference is the presence or absence of the layer of wetting fluid on the channel walls that is discussed later.

A summary of the results obtained for the various flow conditions is presented in Fig. 4a. The immobilized wetting phase is immobile when the viscosity of the oil is greater than the viscosity of water (see the case with $M = 5.10$). For viscosity ratio close to 1, we observe a recirculating motion of the immobilized phase for low Ca and an immobile phase when $Ca > 10^{-4}$. Finally, when the aqueous phase is more viscous than the oil phase, the immobile phase is recirculating for $Ca > 10^{-3}$. The nature of the dissipative events seems to be strongly correlated with the presence of a lubricating wetting film on the channel wall. These results are further discussed in the remainder of the paper.

4.2. Identification of dissipative regimes

We performed drainage experiments for different microchannel geometries that represent several situations of interest in porous systems (see Fig. 1). As for the former series of experiments, we observed different flow regimes according to the fluid properties and flow conditions. Trapping events occur in the presence of a cavity but also up-

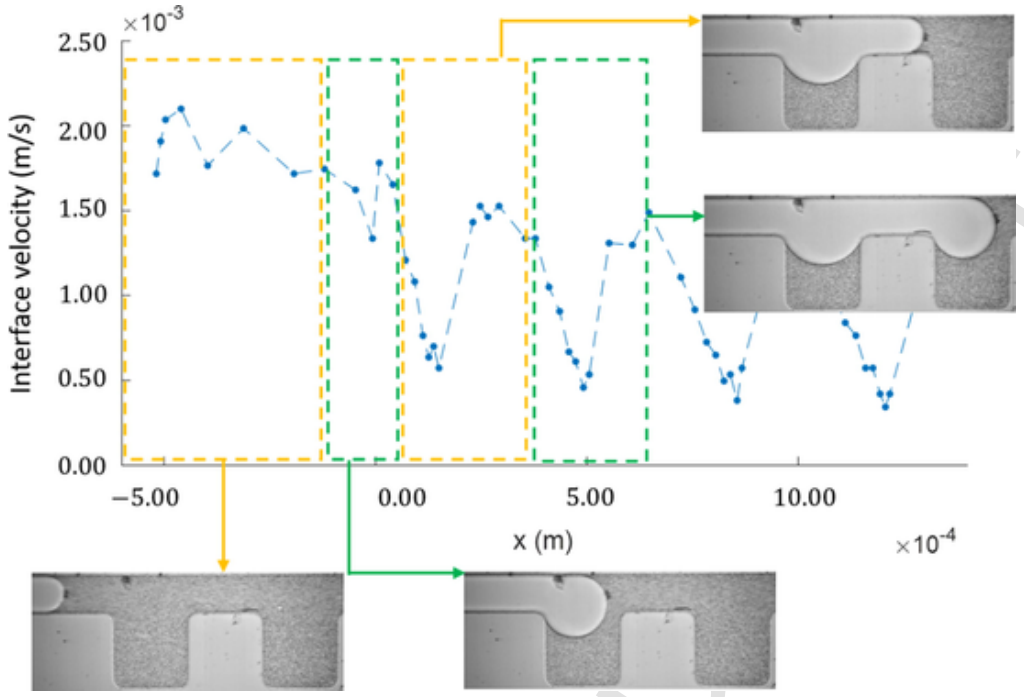

Fig. 3. Interface velocity measurements for $M = 0.09$ (fluid pair 4) and $Ca = 4.70 \times 10^{-3}$. The snapshots show the approximate interface position for each group of measurements, i.e. inlet channel, first pocket, main channel, and second pocket. Interface velocity is measured at the center of the main channel.

stream or downstream a pore-throat constriction (square or smooth) or in a pore-doublet configuration. A summary of the results is shown on Fig. 4. For each trapped globule of wetting phase we report measurements of the velocity of the oil/water interface before trapping, V_o^I, the maximum velocity at the fluid-fluid interface measured by micro-PIV, $\max(u_w)$, the ratio of the oil penetration depth to the eddy pocket size, the total globule viscous dissipation, Φ, the drag force at the fluid-fluid interface, M_{ow}, and the ratio of the fluid-fluid interfacial area to the volume of the water globule. The experimental conditions, *M* and *Ca*, are also displayed, as well as the dissipative regime identified. It appears that viscous dissipation mechanisms are a complex interplay between the geometry of the immobilized phase, viscosity ratio, capillary number and lubrication effect. Overall, we identify four different viscous dissipation regimes based on the internal flows of the trapped globule: an *immobile regime*, a *co-current regime*, a *rim-interface driven regime* and a *lid-cavity driven regime*.

In the *immobile regime* the immobile phase is trapped, does not move and the interface acts as a solid wall. At larger scale, this regime corresponds to the domain of validity of the two-phase Darcy's law with relative permeabilities.

In the *co-current regime*, an elongated wetting phase globule is trapped along the channel walls, Fig. 5a. We observe a co-current flow due to the shear stress at the fluid-fluid interface, even if the body of water looked disconnected and trapped. In the latter case, we observe the presence of flowing films at the channel walls. The water goes in the pocket in the same direction as oil everywhere in the globule and the velocity profile shows an increasing velocity from the channel wall to the oil/water interface. The profile of viscous dissipation, Fig. 5a, shows a maximum at the oil/water interface and is minimum at the channel wall.

In the *rim-globule interface driven* regime, Fig. 5b, the water phase is dragged by the oil that is still flowing and shows an internal recirculation. This regime is characterized by a globule having a fluid-fluid interface area greater than the fluid-solid interface area. The center of mass of the globule is the center of the eddy swirl. This is illustrated by the viscous dissipation profile that shows a maximum value at the center of the globule. We observe the presence of particles flowing through the films at the channel walls for all the cases of the rim-globule interface driven regime.

In the *lid-cavity driven regime*, Fig. 5c, we also observe a recirculating motion. In this case, however, the swirl and the viscous dissipation are localized at the vicinity of the fluid-fluid interface. Indeed, the viscous dissipation profile shows non-zero values only close to the interface. This regime is characterized by a fluid-solid interfacial area greater than the fluid-fluid interfacial area. For this regime, we also observe the presence of moving films.

Interestingly, the viscous dissipation magnitude is in the same order of magnitude for all the experiments (except for the immobile regime), i.e. $\sim 10^{-5}$ m^2/s^3, with capillary numbers varying from 10^{-6} to 10^{-3}. For the dissipative regimes, the drag force M_{ow} varies from 10^{-10} to 10^{-8} Pa m^{-2}. The greatest value (2.61×10^{-8} Pa m^{-2}) is found for the co-current regime when the whole globule is dragged in the direction of the oil flow.

4.3. Discussion

We investigate the effect of the capillary number on the viscous dissipative regime for $M = 0.90$. We observe a recirculating motion within immobile globules for small values of *Ca*, i.e. from $Ca = 9.75 \times 10^{-7}$ to 4.68×10^{-5}, whereas for $Ca = 1.26 \times 10^{-4}$ and 4.34×10^{-4}, the wetting phase is trapped and immobile. When comparing experiments in eddy pocket geometries for $M = 0.90$ (Fig. 4a, two middle pictures), the only parameter that differs significantly between both experiments is the velocity of the oil/water interface and, thus, the capillary number. By looking closely at these two experiments we notice that when a recirculating motion is observed the trapped globule of water is connected to the main flow through liquid films on the channel walls. This wetting layer is present along the whole channel edges. This lubrication effect is visible notably by the shape of the oil-water interface. For $Ca = 7.69 \times 10^{-6}$, there is a momentum transfer at the fluid-fluid interface as well as through liquid films on the channel walls that are subjected to the imposed flow rate in the channel.

a

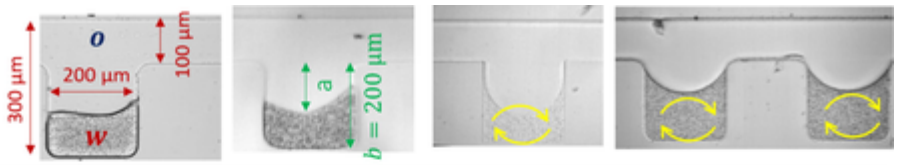

Dissipative regime	Immobile	Immobile	Lid-cavity driven	Lid-cavity driven	
Fluid pair	2	3	3	4	
V_o^I (m/s)	8.30×10^{-5}	1.70×10^{-3}	5.16×10^{-5}	1.45×10^{-3}	
$Ca = \frac{\mu_o \times V_o^I}{\sigma_{ow}}$	2.17×10^{-6}	4.34×10^{-4}	7.69×10^{-6}	4.73×10^{-3}	
$M = \frac{\mu_o}{\mu_w}$	5.10	0.90	0.90	0.09	
$max(u_w)$ at interface ($\times 10^{-5}$ m/s)	0.00	0.00	1.21	2.42	2.49
$\frac{\text{oil depth } (a)}{\text{pocket height } (b)}$	0.56	0.60	0.69	0.41	0.39
Φ ($\times 10^{-5}$ m^2/s^3)	0.00	0.00	0.26	3.03	2.74
M_{ow} ($\times 10^{-9}$ Pa/m^2)	0.00	0.00	4.28	24.88	14.09
Interfacial area / trapped globule volume ($\times 10^4$ m^{-1})	0.94	1.25	2.03	0.98	0.95

b

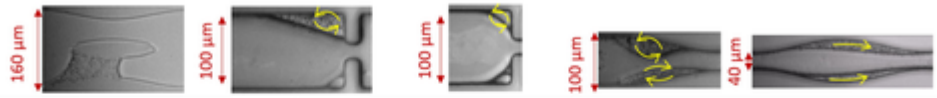

Dissipative regime	Immobile	Rim-globule interface driven	Rim-globule interface driven		Rim-globule interface driven	Co-current
Fluid pair	3	1	1		1	1
V_{ty} (m/s)	8.43×10^{-4}	5.09×10^{-5}	2.44×10^{-5}		9.65×10^{-5}	3.75×10^{-4}
$Ca = \frac{\mu_w \times V_o^I}{\sigma_{ow}}$	1.26×10^{-4}	9.75×10^{-7}	4.68×10^{-5}		1.85×10^{-6}	7.19×10^{-6}
$M = \frac{\mu_o}{\mu_w}$	0.90	0.93	0.93		0.93	0.93
$max(u_w)$ at interface ($\times 10^{-5}$ m/s)	0.00	2.1	3.41	1.83	4.01	1.61
Φ (10^{-5} m^2/s^3)	0.00	0.94	3.34	1.95	0.81	1.60
M_{ow} ($\times 10^{-9}$ Pa/m^2)	0.00	3.41	1.36	0.22	7.54	26.08
Interfacial area / trapped globule volume ($\times 10^4$ m^{-1})	2.02	4.39	6.20	6.41	3.71	5.02

Fig. 4. Summary of the results, (a) eddy pocket geometries, (b) microchannels made of successive pores and pore doublet geometries.

On the contrary, for the case of an immobile pocket, i.e. $Ca = 4.34 \times 10^{-4}$, the oil/water interface is localized at the bottom of the pocket only. This water globule in a dead-end pore does not receive the flow rate imposed in the main channel and the internal flow relies only on the momentum transfer at the fluid/fluid interface. As already discussed, liquid films and flow of particles within them are clearly visible on the channel walls for all dissipative regimes. Thus, we can argue that the lubrication effect is an important parameter to explain whether or not enough momentum is transmitted to the fluid phase to be put in motion. However, it is not clear why the lubrication effect is less important for greater values of *Ca* in the case $M = 0.90$. Indeed, in capillaries of circular cross-section the film thickness increases with *Ca* [21,24]. One hypothesis is that liquid films are present at large *Ca* but the velocity of the interface exerts a force that will completely disconnect the water globule. In other words, the oil interface is so fast that the water film breaks away and once oil is attached to the channel surface it will remain in place.

Besides the case $M = 0.90$, the trapped phase is immobile for $M = 5.10$ at low *Ca*, in this case also the globule looks disconnected from the main channel. This is in agreement with the fact that a lower wetting film thickness is expected for greater viscosity of the oil [51]. This is also in agreement with Dullien [52] who discussed the effect of the viscosity ratio on relative permeabilities. Dullien [52] stated that for low *Ca*, i.e. about 10^{-6} and for a viscosity ratio greater than 1, the lubrication effect is negligible as well as the hydraulic coupling between the wetting and the non-wetting phase. Our results are also in agreement with Yiotis et al. [53] who studied viscous coupling effects during two-phase immiscible flow using a Lattice Boltzmann method. Indeed, Yiotis et al. [53] found that when the wetting fluid is less viscous than the non-wetting fluid then the apparent relative permeability of the non wetting phase may take values greater than unity due to the

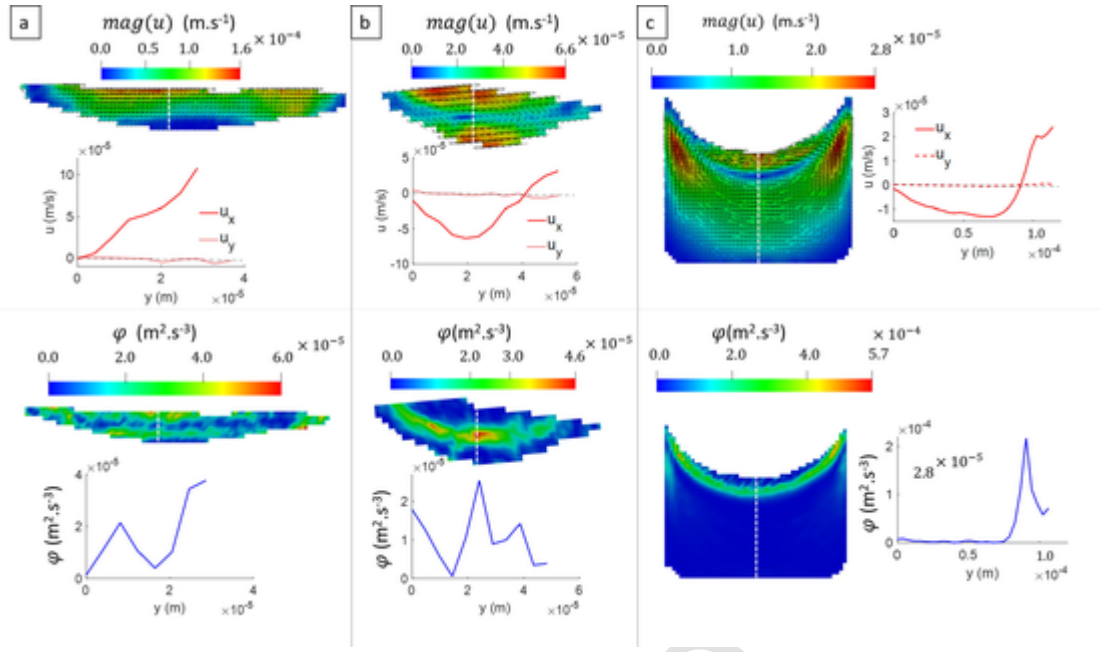

Fig. 5. Illustration of the viscous dissipative regime identified. (a) Co-current regime. (b) Rim-globule interface driven regime. (c) Lid-cavity driven regime. For each regime measurements of the velocity magnitude field, and viscous dissipation field are presented, as well as velocity and viscous dissipation profiles along the white dotted line, from the channel solid wall at $y = 0$ to the fluid-fluid interface.

lubricating effect of the wetting films that cover the solid walls. Consequently, a complete understanding of dissipation mechanisms calls also for an accurate knowledge of lubrication films, as highlighted by Huerre et al. [23] in the context of understanding droplet velocity.

We have seen that the viscous dissipation field, φ, is an important parameter to characterize the viscous dissipation regimes. Therefore, we looked for correlations of the mean viscous dissipation in the globules, Φ, with other experimental parameters. For $M = 0.90$, among all the evaluated parameters, a correlation was found between the intensity of viscous dissipation and the velocity at the fluid-fluid interface linked to the length of the interface. Indeed, Φ varies linearly with the ratio of the velocity at the fluid-fluid interface to the length of the interface, see Fig. 6a, blue squares.

For similar velocity values at the oil-water interface, i.e. about 10^{-5} m/s (Fig. 4), the total viscous dissipation in water globules Φ is greater when the length of the interface is lower, i.e. when the interfacial momentum transfer is concentrated on a smaller area avoiding a significant attenuation of the momentum along the interface. Greater values of Φ are also linked to smaller immobile globules where the whole volume of the globule is recirculating at significant velocities, i.e. rim-globule interface driven regime. As shown in Fig. 4, when the ratio of the interfacial area to the globule volume is greater, i.e. equal to 6.20×10^4, Φ is also greater (3.34×10^{-5}). Thus, as one can expect the interfacial area is an important parameter to quantify viscous dissipative effects and smaller globules tends to dissipate more viscous energy than larger ones.

Regarding the co-current regime (green diamond on Fig. 6), the viscous dissipation is slightly lower than for the other dissipative regimes. This might show that, for similar flow conditions, more viscous energy is dissipated when the immobilized fluid is recirculating than when it is dragged in the direction of the imposed flow. When water is more viscous than oil, i.e. $M = 0.09$, we measured greater values of Φ as shown in Fig. 6a, red circles. The case of $M = 0.09$ corresponds to the experiment where the lubrication effect is the more visible with corner flows of several micrometers in thickness and significant velocity of the particles in the films. This is in agreement with the fact that as the viscosity of the wetting fluid increases, the thickness of the wetting films increases during drainage [51].

On Fig. 6b we also present measurements of the drag force at the fluid-fluid interface, M_{ow}, as a function of the ratio of the velocity at the fluid-fluid interface to the length of the interface. For $M = 0.9, M_{ow}$ is in the same order of magnitude for the lid-cavity and rim-globule interface driven regimes and is greater for the co-current regime. Thus, the interfacial momentum transfer force is greater here when the wetting fluid is dragged in the direction of the imposed flow than when it is recirculating.

The results for $M = 0.9$ highlight that for the co-current regime, less energy is dissipated and more momentum is transferred compared to the other dissipative regimes, resulting in an increase of the mobility of the wetting phase. This is probably linked with the fact that, for similar capillary number (10^{-6}) the velocity at the oil/water interface is greater for the co-current regime than for the other regimes (see Fig. 4). The interfacial momentum transfer is also greater when the wetting fluid is more viscous than the non-wetting one, resulting probably in greater increase in oil mobility.

At a larger scale, the results presented in this paper suggest that viscous coupling is more significant when many small globules of the wetting fluid are immobilized in a porous medium than in the presence of large globules. Thus, further insights into trapping mechanisms are needed. Indeed, the occurrence of trapping will also determine occurrence of viscous dissipation. Moreover, we have shown that, for viscosity ratio close to 1 and low Ca ($<10^{-4}$) the Darcy's extended law for two-phase flows should not neglect the mutual interactions between the fluids. The importance of the viscosity ratio on viscous coupling is also shown. On the one hand the viscosity ratio affects the size of globules formed during drainage, for example when the viscosity of the non-wetting phase is greater, fingering will develop during the invasion and large globules of wetting phase are trapped. On the other hand, the viscosity ratio plays a role on the lubrication films that enhance the transfer of momentum.

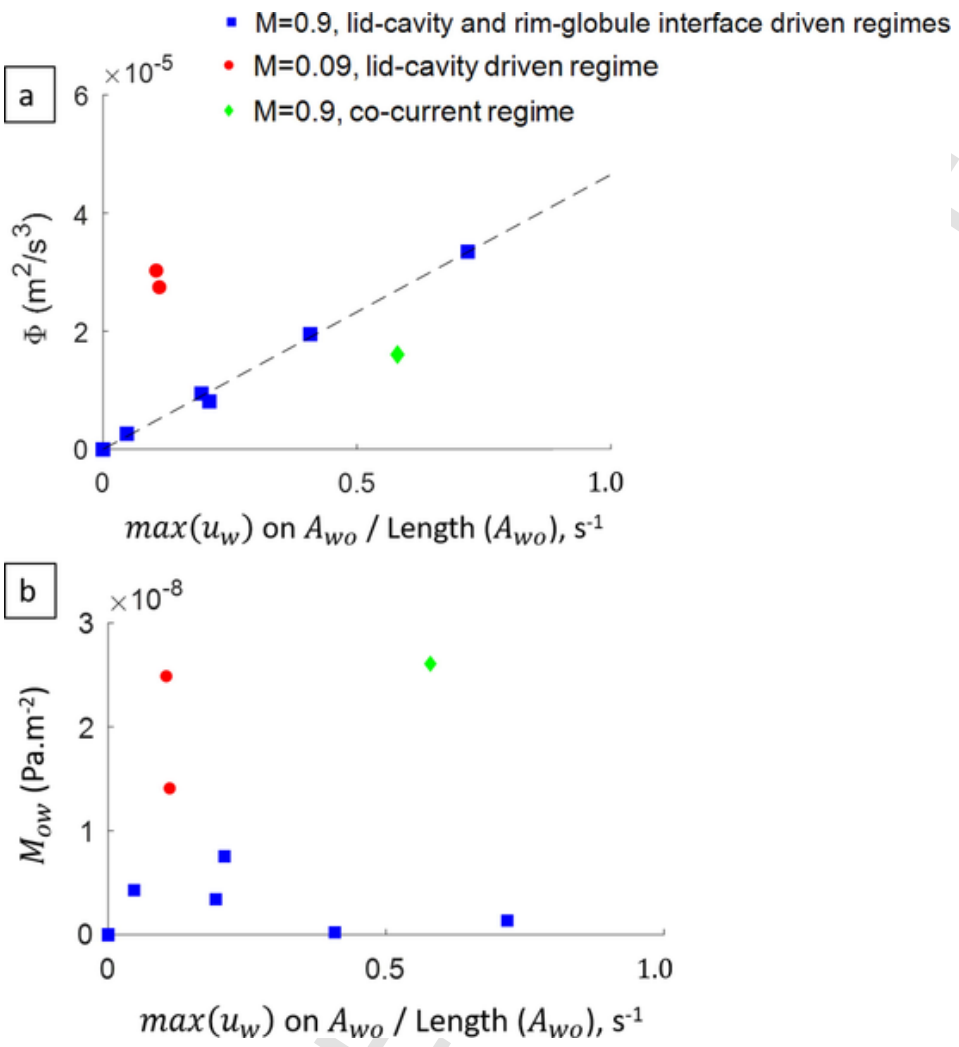

Fig. 6. Viscous dissipation (a) and drag force at the fluid-fluid interface (b) as a function of the ratio of the velocity at the fluid-fluid interface and the interface length. For $M = 0.90$, Φ varies linearly with the ratio $\max(u_w)/A_{wo}$ by a factor 4.65×10^{-5} (dashed line, A).

5. Conclusion

This work has demonstrated that by considering interfacial flow processes at the pore-scale, we are able to assess the significance of viscous coupling effects at larger scale.

A discussion of the theoretical background of continuum-scale models allowed us to identify a generic formulation of the two-phase macroscale model with no speculation on the form of the drag forces unlike previous studies [16,31,37,54]. For the first time, we investigated experimentally the magnitude of the interfacial momentum transfer force for different flow conditions. We performed two-phase flow experiments in micromodels with a focus on observing the flow in immobile pockets of wetting phase. The quantitative measurements obtained using micro-Particle Image Velocimetry (micro-PIV) are unique: velocity field, viscous dissipation rate and shear stress were obtained with high resolution. The experimental results show that after the passage of the oil front during drainage, four regimes of viscous dissipation exist for the globules of water that are immobilized. These regimes depend on macroscale parameters of the flow, on the topology of the pore space, and on the importance of the lubricating effect. These phenomena are highly nonlinear.

At larger scale we identified flow conditions for which the standard two-phase Darcy's law with relative permeabilities is valid, typically when the flowing non-wetting phase is more viscous than the trapped phase, in agreement with Dullien [52]. For viscosity ratio close to 1 and small capillary numbers, the momentum transfer at the fluid-fluid interface is not negligible. Specifically, we demonstrated that viscous dissipation is more important in the case of many small globules of trapped fluids than of large globules of wetting phase. These results are pertinent to the modeling of two-phase flow in porous media, typically CO2 sequestration in geological formations or remediation of ground waters.

The fluids used in this study were free from impurities, however, we can assume that asphaltenes or particulates will change the properties at the fluid-fluid interface in real-world systems. In particular, some authors argue that crude oils give a no slip oil-water interface because they give a rigid interface. Future work should address the effect of impurities on the interface properties and on the momentum transfer at the fluid-fluid interface. Moreover, it will be worthwhile to study the effect of dissipative processes on transport properties. Indeed, the recirculating motion in immobile wetting phase globules could enhance mixing [55] or dissolution processes.

Acknowledgements

This work has received support from the French Agency for Research (Agence Nationale de la Recherche, ANR) through the grant CONGE BLAN-610-01, the Equipex Planex ANR-11-EQPX-36 and the

labex Voltaire ANR-10-LABX-100-01. This work was supported partially by the Stanford University Petroleum Research Institute (SUPRIA) as well as the Stanford Nano Shared Facilities (SNSF) through the National Science Foundation, award ECCS-1542152. SR gratefully acknowledge R. Dussart, M. Kulsreshath, P. Lefaucheux, and the CERTeM for their participation on microfabrication. CS was funded by the BRGM RDI TRIPHASIQUE project.

Appendix A. Supplementary material

Supplementary data associated with this article can be found, in the online version, at https://doi.org/10.1016/j.jcis.2019.09.072.

References

[1] M. Riazi, M. Sohrabi, C. Bernstone, M. Jamiolahmady, S. Ireland, Visualisation of mechanisms involved in CO_2 injection and storage in hydrocarbon reservoirs and water-bearing aquifers, Chem. Eng. Res. Des. 89 (2011) 1827–1840.
[2] W. Yun, A. Kovscek, Microvisual investigation of polymer retention on the homogeneous pore network of a micromodel, J. Petrol. Sci. Eng. 128 (2015) 115–127.
[3] C. Zhang, C.J. Werth, A.G. Webb, Characterization of napl source zone architecture and dissolution kinetics in heterogeneous porous media using magnetic resonance imaging, Environ. Sci. Technol. 41 (2007) 3672–3678 PMID: 17547195.
[4] P. Sapin, A. Gourbil, P. Duru, F. Fichot, M. Prat, M. Quintard, Reflooding with internal boiling of a heating model porous medium with mm-scale pores, Int. J. Heat Mass Transf. 99 (2016) 512–520.
[5] C. Soulaine, P. Horgue, J. Franc, M. Quintard, Gas-liquid flow modeling in columns equipped with structured packing, AIChE J. 60 (2014) 3665–3674.
[6] M. Muskat, Physical Principles of Oil Production, McGraw-Hill Ed., New York, 1949.
[7] M. Danis, M. Quintard, Modélisation d'un écoulement diphasique dans une succession de pores, Oil & Gas Sci. Technol. 39 (1984) 37–46.
[8] W. Rose, Myths about later-day extensions of darcy's law, J. Petrol. Sci. Eng. 26 (2000) 187–198.
[9] Y. Cinar, A. Riaz, H.A. Tchelepi, Experimental study of CO_2 injection into saline formations, SPE J. 14 (2009) 588–594.
[10] S.A. Aryana, A.R. Kovscek, Experiments and analysis of drainage displacement processes relevant to carbon dioxide injection, Phys. Rev. E 86 (2012).
[11] Y. Méheust, G. Løvoll, K. Måløy, K. Jørgen, J. Schmittbuhl, Interface scaling in a two-dimensional porous medium under combined viscous, gravity, and capillary effects, Phys. Rev. E 66 (2002) 51603.
[12] C. Zarcone, R. Lenormand, Determination experimentale de couplage visqueux dans les ecoulements diphasiques en milieu poreux, C.R. Acad. Sci. Paris Serie II (1994) 1429–1438.
[13] J. Nordbotten, M. Celia, S. Bachu, Injection and storage of CO_2 in deep saline aquifers: Analytical solution for CO_2 plume evolution during injection, Transp. Porous Media 58 (2005) 339–360.
[14] V. Kumbar, P. Dostal, Temperature dependence density and kinematic viscosity of petrol, bioethanol and their blends, Pakistan J. Agric. Sci. 51 (2014) 175–179.
[15] C.H. Byers, D.F. Williams, Viscosities of pure polyaromatic hydrocarbons, J. Chem. Eng. Data 32 (1987) 344–348.
[16] R. Ehrlich, Viscous coupling in two-phase flow in porous media and its effect on relative permeabilities, Transp. Porous Media 11 (1993) 201–218.
[17] W. Rose, Fluid flow in petroleum reservoirs: Iii. effect of fluid-fluid interfacial boundary condition, Illinois State Geol. Surv. Circ. 291 (1960) 1–18.
[18] M. Pilotti, S. Succi, G. Menduni, Energy dissipation and permeability in porous media, EPL (Europhys. Lett.) 60 (2002) 72.
[19] M. Ayub, R.G. Bentsen, Experimental testing of interfacial coupling in two-phase flow in porous media, Pet. Sci. Technol. 23 (2005) 863–897.
[20] G. Taylor, Deposition of a viscou fluid on the wall of a tube, J. Fluid Mech. 10 (1961) 161–165.
[21] F.P. Bretherton, The motion of long bubbles in tubes, J. Fluid Mech. 10 (1961) 166–188.
[22] S. Hodges, O. Jensen, J. Rallison, The motion of a viscous drop through a cylindrical tube, J. Fluid Mech. 501 (2004) 279–301.
[23] A. Huerre, O. Theodoly, A.M. Leshansky, M.-P. Valignat, I. Cantat, M.-C. Jullien, Droplets in microchannels: Dynamical properties of the lubrication film, Phys. Rev. Lett. 115 (2015) 64501.
[24] S. Roman, M.O. Abu-Al-Saud, T. Tokunaga, J. Wan, A.R. Kovscek, H.A. Tchelepi, Measurements and simulation of liquid films during drainage displacements and snap-off in constricted capillary tubes, J. Colloid Interface Sci. 507 (2017) 279–289.
[25] Y. Kim, J. Wan, T.J. Kneafsey, T.K. Tokunaga, Dewetting of silica surfaces upon reactions with supercritical CO_2 and brine: Pore-scale studies in micromodels, Environ. Sci. Technol. 46 (2012) 4228–4235.
[26] S.S. Datta, T.S. Ramakrishnan, D.A. Weitz, Mobilization of a trapped non-wetting fluid from a three-dimensional porous medium, Phys. Fluids 26 (2014) 22002.
[27] C.I. Steefel, S. Molins, D. Trebotich, Pore scale processes associated with subsurface CO_2 injection and sequestration, Rev. Mineral. Geochem. 77 (2013) 259–303.
[28] S. Roman, C. Soulaine, M.A. AlSaud, A. Kovscek, H. Tchelepi, Particle velocimetry analysis of immiscible two-phase flow in micromodels, Adv. Water Resour. 95 (2016) 199–211.
[29] M. Heshmati, M. Piri, Interfacial boundary conditions and residual trapping: A pore-scale investigation of the effects of wetting phase flow rate and viscosity using micro-particle image velocimetry, Fuel 224 (2018) 560–578.
[30] I. Zarikos, A. Terzis, S. Hassanizadeh, B. Weigand, Velocity distributions in trapped and mobilized non-wetting phase ganglia in porous media, Sci. Rep. 8 (2018) 13228.
[31] D. Avraam, A. Payatakes, Generalized relative permeability coefficients during steady-state two-phase flow in porous media, and correlation with the flow mechanisms, Transp. Porous Media 20 (1995) 135–168.
[32] C. Marle, On macroscopic equations governing multiphase flow with diffusion and chemical reactions in porous media, Int. J. Eng. Sci. 20 (1982) 643–662.
[33] F. Kalaydjian, A macroscopic description of multiphase flow in porous media involving spacetime evolution of fluid/fluid interface, Transp. Porous Media 2 (1987) 537–552.
[34] S. Hassanizadeh, W.G. Gray, Mechanics and thermodynamics of multiphase flow in porous media including interphase boundaries, Adv. Water Resour. 13 (1990) 169–186.
[35] P.A.C. Raats, A. Klute, Transport in soils: The balance of momentum, Soil Sci. Soc. Am. J. 32 (1968) 452–456.
[36] P. Baveye, G. Sposito, The operational significance of the continuum hypothesis in the theory of water movement through soils and aquifers, Water Resour. Res. 20 (1984) 521–530.
[37] F. Kalaydjian, Origin and quantification of coupling between relative permeabilities for two-phase flows in porous media, Transp. Porous Media 5 (1990) 215–229.
[38] D. Lasseux, M. Quintard, S. Whitaker, Determination of permeability tensors for two-phase flow in homogeneous porous media: Theory, Transp. Porous Media 24 (1996) 107–137.
[39] J. Bear, Dynamics of Fluids in Porous Media, Elsevier, New York, 1972.
[40] W. Rose, Measuring transport coefficients necessary for the description of coupled two-phase flow of immiscible fluids in porous media, Transp. Porous Media 3 (1988) 163–171.
[41] F.A.L. Dullien, M. Dong, Experimental determination of the flow transport coefficients in the coupled equations of two-phase flow in porous media, Transp. Porous Media 25 (1996) 97–120.
[42] H. Li, C. Pan, C.T. Miller, Pore-scale investigation of viscous coupling effects for two-phase flow in porous media, Phys. Rev. E 72 (2005) 26705.

[43] M. Shams, A.Q. Raeini, M.J. Blunt, B. Bijeljic, A study to investigate viscous coupling effects on the hydraulic conductance of fluid layers in two-phase flow at the pore level, J. Colloid Interface Sci. 522 (2018) 299–310.
[44] J. Hornbrook, L. Castanier, P. Pettit, Observation of foam/oil interactions in a new, high-resolution micromodel, in: Society of Petroleum Engineers, 1991.
[45] M. Buchgraber, M. Al-Dossary, C. Ross, A. Kovscek, Creation of a dual-porosity micromodel for pore-level visualization of multiphase flow, J. Petrol. Sci. Eng. 86–87 (2012) 27–38.
[46] S. Tan, N. Nguyen, Y. Chua, T. Kang, Oxygen plasma treatment for reducing hydrophobicity of a sealed polydimethylsiloxane microchannel, Biomicrofluidics 4 (2010).
[47] C. Zhang, M. Oostrom, T.W. Wietsma, J.W. Grate, M.G. Warner, Influence of viscous and capillary forces on immiscible fluid displacement: Pore-scale experimental study in a water-wet micromodel demonstrating viscous and capillary fingering, Energy & Fuels 25 (2011) 3493–3505.
[48] W. Thielicke, E.J. Stamhuis, PIVlab – time-resolved digital particle image velocimetry tool for matlab, 2014.
[49] L. Fiabane, M. Gohlke, O. Cadot, Characterization of flow contributions to drag and lift of a circular cylinder using a volume expression of the fluid force, Eur. J. Mech. B. Fluids 30 (2011) 311–315.
[50] Y. Liu, J.S. Wexler, C. Schönecker, H.A. Stone, Effect of viscosity ratio on the shear-driven failure of liquid-infused surfaces, Phys. Rev. Fluids 1 (2016) 74003.
[51] J. Chen, D. Wilkinson, Pore-scale viscous fingering in porous-media, Phys. Rev. Lett. 55 (1985) 1892–1895.
[52] F. Dullien, 5 - multiphase flow of immiscible fluids in porous media, in: F. Dullien (Ed.), Porous Media (Second Edition), second ed., Academic Press, San Diego, 1992, pp. 333–485.
[53] A.G. Yiotis, J. Psihogios, M.E. Kainourgiakis, A. Papaioannou, A.K. Stubos, A lattice boltzmann study of viscous coupling effects in immiscible two-phase flow in porous media, Colloids Surf., A 300 (2007) 35–49 Proceedings of the Fourth International TRI/Princeton Workshop..
[54] W. Rose, Coupling coefficients for two-phase flow in pore spaces of simple geometry, Transport Porous Media 10 (1993) 293–296.
[55] J. Maes, C. Soulaine, A new compressive scheme to simulate species transfer across fluid interfaces using the volume-of-fluid method, Chem. Eng. Sci. 190 (2018) 405–418.